Digital Twin-Based Deterioration Prognosis of Steel Wind Turbine Towers in Modular Energy Islands

Heng, Junlin; Zhang, Jiaxin; Kaewunruen, Sakdirat; Dong, You; Baniotopoulos, Charalampos

DOI:
10.1002/cepa.2573

Document Version
Publisher's PDF, also known as Version of record

Citation for published version (Harvard):
Heng, J, Zhang, J, Kaewunruen, S, Dong, Y & Baniotopoulos, C 2023, 'Digital Twin-Based Deterioration Prognosis of Steel Wind Turbine Towers in Modular Energy Islands', *ce/papers*, vol. 6, no. 3-4, pp. 1111-1118. https://doi.org/10.1002/cepa.2573

ce/papers Proceedings in civil engineering

Ernst & Sohn A Wiley Brand

ORIGINAL ARTICLE

eurosteel AMSTERDAM 2023

Ernst & Sohn A Wiley Brand

Digital Twin-Based Deterioration Prognosis of Steel Wind Turbine Towers in Modular Energy Islands

Junlin Heng[1,2] | Jiaxin Zhang[3] | Sakdirat Kaewunruen[1] | You Dong[3]| Charalampos Baniotopoulos[1]

Correspondence

Prof. Charalampos Baniotopoulos
University of Birmingham
School of Engineering
Edgbaston
B15 2TT Birmingham
Email: c.baniotopoulos@bham.ac.uk

[1] University of Birmingham, Birmingham, United Kingdom
[2] Shenzhen University, Shenzhen, China
[3] The Hong Kong Polytechnic University, Hong Kong, China

Abstract

The Modular Energy Island (MEI) offers a promising solution to unlock the plentiful Aeolian source at deep-waters. Meanwhile, high-speed wind and strong corrosivity in the harsh marine environment, along with increasing dynamics, escalate the corrosion-fatigue (C-F) deterioration issue of steel wind turbine towers on MEIs notably. Thus, a better understanding of the C-F states is of particular concern to maximize the lifetime power generation and minimize operational costs. This study aims to provide novel insights into the C-F deterioration states of wind turbine towers by integrating the material test data, site measurement, and multi-physics simulation based on the concept of digital twins. The DTU 10MW reference turbine has been selected as an engineering prototype. Based on the in-situ wind-wave data, the structural response of the steel turbine tower at critical details is predicted via multi-physics simulations and accordingly, stress spectra are constructed. Besides, the corrosion rate is estimated from material test data and the site-specific climate conditions. Then, a probabilistic C-F model is established for the deterioration state of critical components in the tower by incorporating the derived stress spectra and corrosion rate. Not only does this study highlight the escalating C-F deterioration issue in steel wind turbine towers, but it also offers a novel basis for crucial insights into the digital twin-based operation and maintenance (O&M) of the next-generation MEIs by integrating models and data from various sources.

Keywords

Modular Energy Island, Wind Turbine Tower, Corrosion Fatigue, Digital Twin, Wind-Wave, Multi-Physics Simulation.

1 Introduction

The EU Green Deal pledged to a clean, sustainable and carbon-neutral economy powered by renewable energies[1][2]. Along with the escalating global energy crisis, the offshore wind power is becoming even crucial due to its matureness, feasibility and robustness. For instance, the EU has announced plans for 25 times increase in Offshore Wind by 2050, demanding rooted innovation in Wind Energy[3][4]. Moreover, UK plans to increase the offshore wind capacity to an ambitious goal of 50 GW by 2030[5]. Thus, the concept of modular energy island (MEI)[6] is proposed as a promising solution to exploit the plentiful and stable wind source at deep-waters, combined with other types of renewable energies, as shown in Figure 1. Compared with the traditional wind farm, the wind turbine tower on MEIs exposes to the coupled deterioration of load-induced fatigue and environment-assisted corrosion, i.e., the corrosion fatigue (C-F) [7].

As a matter of factor, wind turbine towers are highly prone to wind-induced fatigue at critical connections [8][9]. Thus, sudden and premature fracture will be further risked in floating wind turbine towers due to excessive C-F deterioration after exploitation for years. Especially, if the connection is at the critical point, the C-F failure may lead to serious incidents, such as the Collapse of Alexander Kielland offshore platform [18]. To sum, corrosion fatigue posts challenges on the structural integrity of MEIs and controlling their service life.

Real-time monitoring of wind-wave loads on FOWT structures becomes gradually possible with the implementation of emerging measurement tools such as the floating LiDAR [10]. This offers a promising possibility for digital twin (DT) [11] of deteriorating FOWT structures. The concept of DT originates from the automotive and manufacturing industries, which means integrating physical entities into the digital space [12]. In the civil sector, DT can be regarded as a development from building information modelling (BIM) to explore add-values of data, with further emphasis on the interoperability between physical and digital via data flows [13]. Apart from the general concept, DT in

https://doi.org/10.1002/cepa.2573 wileyonlinelibrary.com/journal/cepa

practice can be approached with various focuses, e.g., design [14], construction [15], prognosis [16] and management [17]. Although the framework of DT is becoming mature as evidenced by the above efforts, a compelling need still exists in the site data-based deterioration prognosis tailored to FOWT structures, which is the core pillar of the deterioration-focused DT. Thus, an effective and dynamic prognosis approach is deemed essential to achieve a better understanding of the up-to-date and future deterioration state of the wind turbine towers on MEIs, by integrating the site-specific data in a DT-based manner.

The present work devotes to provide novel insights into the corrosion fatigue deterioration of floating wind turbine towers, by integrating measured data and theoretical models via a digital twin-based approach. The following context is organised as below: section 2 illustrates the general methodology framework of the digital twin-based prognosis, including the mechanism modelling, multi-physics simulation and corrosion estimation; The major findings are discussed in section 3. Finally, key conclusions are drawn in section 4, along with future suggestions.

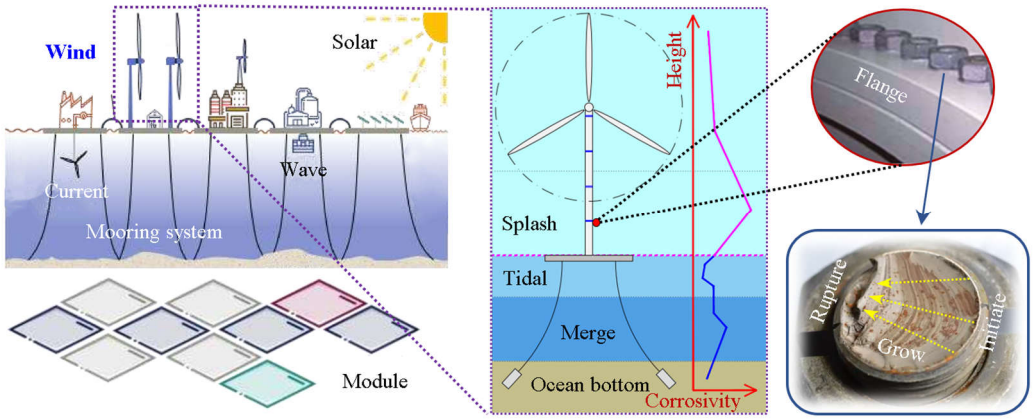

Figure 1 Corrosion-fatigue coupled deterioration of bolts in wind turbine towers on Modular Energy Islands (MEIs)[6][19]

2 Methodology: digital twin-based prognosis

2.1 Probabilistic corrosion fatigue model

As indicated in Fig. 1, high-strength bolts in ring-flanges of the wind turbine tower are highly prone to cracking and fracture as it exposed to the C-F coupled deterioration [20]. High-strength bolts in ring-flanges demonstrates three major potential failure sites under fatigue loading [21], i.e., the head-to-shank radius (Mode-1), root of the first engaged thread (Mode-2) and run-off of threads (Mode-3). As suggested by [22], in case of the in-air fatigue loading, the possibility of occurrence is respectively 0.15, 0.2 and 0.65 in the Mode-1, Mode-2 and Mode-3. Thus, a probabilistic corrosion fatigue (PCF) model is proposed, as shown in Figure 2.

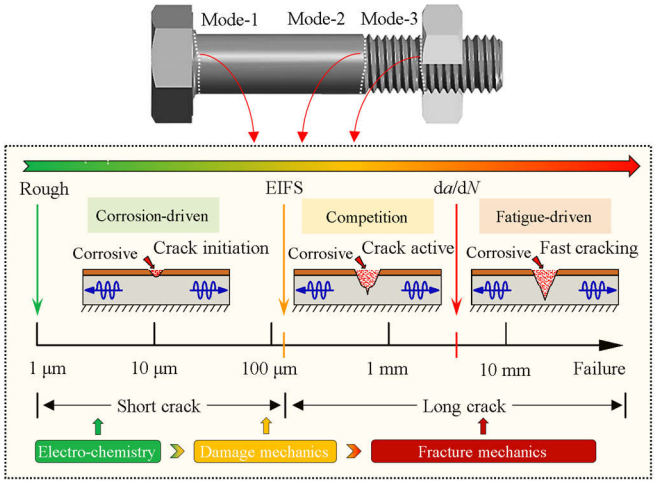

Figure 2 Probabilistic corrosion-fatigue model

In general, the corrosion fatigue evolution could be divided into three stages according to the cracking-driven force, size and growth rate of the crack [23][24]. In the first stage, the crack initiates from initial flaws at the micron-level. Due to the limited crack size, crack growth rate (CGR) is mainly controlled by the corrosion effect. Thus, the first stage is termed as the corrosion-driven stage. Meanwhile, fatigue still imposes a secondary effect in assisting the crack growth. For conservative purpose, a superposition of the two driven forces is assumed in solving crack growth rate of Stage 1[25], as illustrated in Equation 1:

$$\frac{da_{S1}}{dt} = \left(\frac{da_{S1}}{dt}\right)_{co} + \left(\frac{da_{S1}}{dt}\right)_{fa} \qquad (1)$$

Where a_{S1} denotes the crack size in Stage 1; t stands for the service life; the subscript "*co*" and "*fa*" represent the crack growth rate by corrosion and fatigue, respectively.

Since the crack size in Stage 1 is far-below the effective initial flaw size (EIFS) [26], the classic fracture mechanics fails to offer an acceptable prediction of the crack growth rate without dedicate considerations of small cracks. Alternative, the equivalent crack growth rate is estimated by the damage rate solved from the probability-stress-life (P-S-N) model and assumption of linear damage accumulation[27], as illustrated in Equation 2:

$$\left(\frac{da_{S1}}{dt}\right)_{fa} = \frac{d}{dt}\left(\frac{1}{f}\cdot\sum_i \frac{n_i}{[N_i]}\right) \qquad (2)$$

where n_i and $[N_i]$ are applied and allowance number of cycles at a specific stress range, respectively; f denotes the loading frequency.

As the crack reaches the EIFS, the fatigue-driven crack growth rate can be predicted by fracture mechanics effectively [28]. The calculation of the EIFS can be determined

after the crack initiation limit $[\Delta\sigma_{in}]$ and the crack growth threshold $[\Delta K_{th}]$ according to [28]. The C-F evolution then comes into Stage 2, i.e., competition. The crack growth rate will be controlled by the maximum effect between the corrosion and fatigue, as illustrated in Equation 3:

$$\frac{da_{S2}}{dt} = \max\left[\left(\frac{da_{S2}}{dt}\right)_{co}, \left(\frac{da_{S2}}{dt}\right)_{fa}\right] \quad (3)$$

It is worth stating that the acceleration in fatigue by corrosion should be included [29], which will be discussed in details later. With the further development of cracks, the escalating fatigue effect gradually surpass the declining corrosion effect. Accordingly, the C-F evolution steps into Stage 3 (i.e., fatigue-driven phase) until the final failure of bolts. In addition, the same method illustrated in Equation 3 can still be employed for Stage 3.

As noted in Equation 2, the fatigue-induced crack growth rate is determined as the fatigue damage rate for crack initiation. The allowable number of cycles N_i could be determined after the tri-linear P-S-N model [27][29], as illustrated in Equation 4:

$$N_i = \begin{cases} N_D \cdot \left(\frac{[\Delta\sigma_D]}{\Delta\sigma_i}\right)^3, \forall \Delta\sigma_i > [\Delta\sigma_D] \\ N_D \cdot \left(\frac{[\Delta\sigma_D]}{\Delta\sigma_i}\right)^5, \forall [\Delta\sigma_{in}] < \Delta\sigma_i < [\Delta\sigma_D] \\ N_L \cdot \left(\frac{[\Delta\sigma_{in}]}{\Delta\sigma_i}\right)^{22}, \forall \Delta\sigma_i < [\Delta\sigma_{in}] \end{cases} \quad (4)$$

Where $\Delta\sigma_i$ is the applied stress range; N_L is the constant life limit for fatigue crack initiation (i.e., 10^8), corresponding to $[\Delta\sigma_{in}]$; N_D and $[\Delta\sigma_D]$ are the first inflection point at 5×10^6 cycles and associated fatigue strength, respectively.

It is worth stating that the reference strengths are dependent, as illustrated in Equation 5:

$$[\Delta\sigma_D] = \sqrt[5]{100/5} \cdot [\Delta\sigma_L] = 1.82[\Delta\sigma_L] \quad (5)$$

As aforementioned, the fatigue-induced crack growth rate can be solved by fracture mechanics after Stage 1. Accordingly, the modified Paris law [29] is applied to estimate the crack growth rate, as illustrated in Equation 6:

$$\left(\frac{da_{S2,3}}{dt}\right)_{fa} = A_{fcg} \cdot (\Delta K_i - [\Delta K_{th}])^3 \quad (6)$$

where A_{fcg} is the material constant of fatigue crack growth (FCG); ΔK_i denotes the variation in stress intensity factors (SIFs) by the applied stress range; $[\Delta K_{th}]$ is the FCG threshold, below which the crack arrest occurs.

Moreover, as aforementioned, it is crucial to incorporate the acceleration in fatigue by corrosion. According to IIW [29], the material constant A_{fcg} should be multiplied by a factor of 3 in marine environment. In this study, the influence of corrosivity on FCG is further refined in line with the classification of environment in ISO 9223 [30].The modified material constant A'_{fcg} is solved by Equation 7:

$$A'_{fcg} = A_{fcg} \cdot (1 + 2 \cdot \frac{r_{co}}{r^0_{co}}) \quad (7)$$

where r_{co} is the environmental corrosivity expressed in terms of first-year corrosion of carbon steels ($\mu m/yr$); r^0_{co} is the benchmark value of r_{co} at the C5 (very high corrosion) environment, i.e., 200 $\mu m/yr$ [30].

The variation in SIFs ΔK_i can be solved from the applied stress range $\Delta\sigma_i$, as illustrated in Equation 8:

$$\Delta K_i = Y_{fcg} \cdot \Delta\sigma_i \sqrt{\pi a_i} \quad (8)$$

where a_i stands for the crack depth; Y_{fcg} is the crack size-related correction factor, of which the solution for crack in bolts can be found from [31].

As discussed in Section 2.1, the high-strength bolt has three different fatigue-critical sites and then demonstrates three failure modes. In order to contain the contribution of all the three modes within a probabilistic framework, a parallel system is proposed for the failure assessment diagram (FAD) of bolts, as shown in Figure 3. Thus, the failure of bolts is assumed once the failure criteria is achieved in any of the three modes. Accordingly, the failure probability of bolts can be solved as Equation 9:

$$P_{f,blt}(t) = 1 - \prod_{i=1}^{3}(1 - P_{f,i}(t)) \quad (9)$$

Where $P_{f,blt}(t)$ stands for the failure probability of bolts at time t; $P_{f,i}(t)$ is the failure probability of the i-th mode.

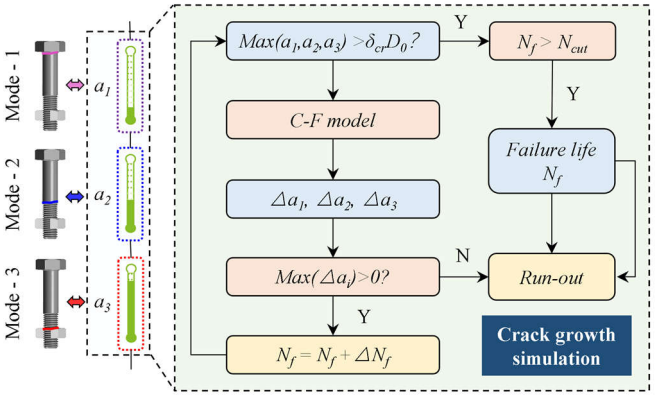

Figure 3 Failure assessment diagram (FAD) and computational procedures of high-strength bolts under corrosion fatigue deterioration.

In addition, the failure probability of each mode $P_{f,i}(t)$ can be determined by the limit stage function (LSF) considering the critical crack size, as illustrated in Equation 10:

$$P_{f,i}(t) = Prob[D_0 - a_i(t) < 0] \quad (10)$$

where $a_i(t)$ is the crack depth in the i-th mode; D_0 is critical crack depth, determined as 65% of the effective bolt diameter according to [31].

Accordingly, Monte Carlo (MC)-based sampling can be carried out to generate essential numerical samples for the simulation of the PCG model. Each sample can be then solved in a deterministic manner step-by-step, as shown by the flowchart in Figure 3. It is worth stating that, for numerical practicality, a cut-off limit is imposed on the maximum number of cycles, i.e., 10^{10} in this work.

2.2 Corrosion modelling and estimation

The corrosion loss in the thickness D_{co} is estimated via the

power function model suggested in ISO 9224 [32], as illustrated in Equation 10:

$$D_{co} = r_{co} \cdot t^{\beta} \qquad (11)$$

where β is the material related power index.

As aforementioned, the first-year corrosion loss of carbon steel, denoted as r_{co}, reflects the environmental corrosivity. The parameter can be derived according to the empirical model suggested in ISO 9223 [33], as illustrated in Equation 11:

$$r_{co} = 1.77 \cdot P_d^{0.52} \cdot e^{0.02RH + f_{st}} + 0.102 \cdot S_d^{0.62} \cdot e^{0.033RH + 0.04T} \quad (11a)$$

$$f_{st} = \begin{cases} 0.15 \cdot (T-10), \forall T \le 10℃ \\ -0.054 \cdot (T-10), \forall T > 10℃ \end{cases} \qquad (11a)$$

where P_d is the average SO_2 deposition (in $mg/m^2/day$); RH is the average relative humidity (in %); S_d is the average Cl^- deposition (in $mg/m^2/day$); T is the average temperature (in ℃).

In this study, the Gulf of Mexico is considered as typical application site of MEIs. Accordingly, the climate condition is determined via the site-specific measurement [34], as shown in Table 1.

Table 1 Climate condition under investigation (adapted from [34])

Parameter	Unit	Value
P_d	$mg/m^2/day$	7.3
RH	%	86.0
S_d	$mg/m^2/day$	312.0
T	℃	20.6

The material-related index β is still left to be determined. Thus, the data from the free corrosion test of Q235-steel coupons have been employed [35], as illustrated in Figure 4. Meanwhile, as indicated by the PCF model in Figure 2, pitting corrosion is much detrimental than the general corrosion loss D_{co}. Accordingly, the ratio of pit depth to general corrosion is determined as 2.0 according to the statistics by [36].

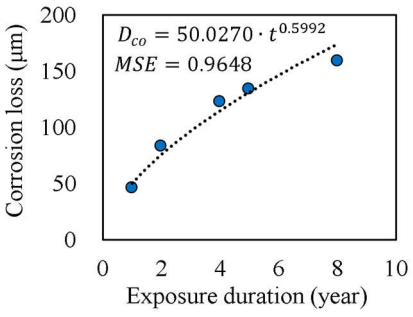

Figure 4 Regression model for general corrosion loss in Q235-steel

As a result, the depth of corrosion pits in the investigating environment can be predicted by Equation 12:

$$a_{pit}(t) = 509.8390 \cdot t^{0.5992} \qquad (12)$$

where a_{pit} denote the depth of corrosion pits at time t.

2.3 Fatigue stress by hybrid simulations

Apart from corrosion rate, Fatigue stress in bolts is another crucial factor controlling the C-F evolution, which may be even more important. Similarly, the site-specific measurement data by NDBC [34] are also employed in modelling the wind-wave distribution, as shown in Figure 5.

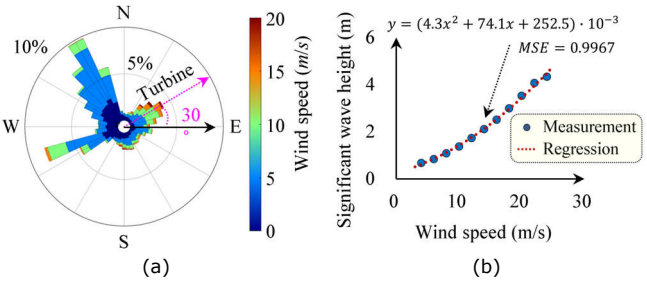

Figure 5 Wind-wave model by site measurement: (a) wind rose; (b) wind-wave correlation. (Adapted from [34])

As indicated in Figure 5b, a very strong correlation exists between the wind speed and wave height. Thus, the uncertainties in the wind are incorporated via the wind rose shown in Figure 5a, while the wave height is assumed as a dependent value via the correlation model shown in Figure 5b.

The DTU 10MW reference turbine [37] is selected for the case study, in accordance to a floating platform anchored to the seabed by mooring chains proposed in [38]. The diameter of the 115.63 m-tall tower ranges from 8.30 m at the base to 5.50 m at the hub, with the thickness ranging from 38 mm to 20 mm. In order to fully exploit the wind source, the turbine is oriented along with the winds, i.e., 30 degrees east by north. The multi-physics system OpenFAST [39] is leveraged to model the wind turbine system as a whole, including the turbine, tower, floating platform and mooring chains, as shown in Figure 6.

Figure 6 Muti-physics simulation modelling by OpenFAST

Accordingly, the time history of structural responses (e.g.,

sectional forces) can be derived from the muti-physics simulation based on a specific wind speed-wave height. After a further transform from the sectional force to bolt stress by load transfer function [40], the stress history in bolts can be derived. Then, using cycle-counting approaches (e.g., the rain-flow method [41]), the stress spectra can be derived for various wind-wave conditions. Based on the probabilistic wind-wave distribution in Figure 5, the general stress spectra can be established, as illustrated by Equation 13:

$$P(\Delta\sigma_i) = P(\Delta\sigma_i|v_w, h_v) \cdot P(v_w, h_v) \qquad (12)$$

Where $P(\Delta\sigma_i)$ standards for the probability of stress range $\Delta\sigma_i$ in the total distribution; $P(\Delta\sigma_i|v_w, h_v)$ is the probability of $\Delta\sigma_i$ conditional on the wind speed v_w and significant wave height h_v; $P(v_w, h_v)$ is joint probability of v_w and h_v shown in Figure 5.

Figure 7 shows the final stress spectra of the critical bolt in the ring-flange connection, of which the detailed location will be discussed later. Obviously, the probability mass decreases rapidly with the increase in the stress level. However, as a common practice, the high-stress region of small probabilities will contribute much more notably to the deterioration comparing with the low-stress region.

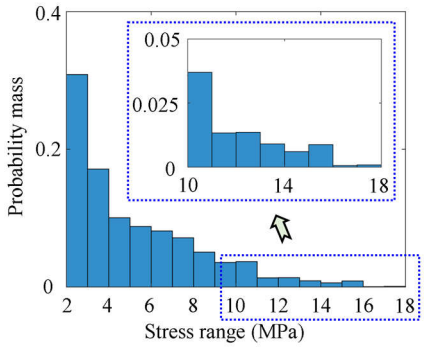

Figure 7 Fatigue strength spectra of the critical bolt in the ring-flange

3 Results and discussion

Based on the methodology illustrated in Section 2, probabilistic prognosis can be carried out on the corrosion fatigue evolution of bolts by integrating the site-specific loads and climate conditions. According to the result, the design life of the critical bolt is 19.2 years under the given condition. Figure 8a shows the damage of bolts (i.e., 25 representatives selected out of 150 bolts) at the bottom flange of the tower, after exploited for 19.2 years. In order to incorporate uncertainties in the probabilistic simulation, the damage is expressed in terms of the characteristic value at the survival rate of 97.7% [29]. The result indicates a strong correlation between the bolt damage and wind direction. For instance, the critical region can be identified at the upwind region of strong winds, which is also the direction of the turbine (in order to maximise the power production).

The critical region is further visualised in details in terms of the expected design life, as shown in Figure 8b. Apparently, a list of bolts around the critical bolt is prone to premature failure before the design life of 25 years. As a result, special attentions are suggested for bolts in the upwind direction of strong winds, in both the design, manufacturing and maintenance.

As aforementioned, the high-strength bolt shows a total of three failure modes. Thus, a further investigation is conducted on the proportion of failure modes and associated evolution of probability distribution of the maximum crack depth, as shown in Figure 9b. The highest failure probability of 74.7% achieves under Mode-3, followed by Mode-1 of 20.3%, while Mode-2 shows the lowest probability of 5%. Recalling the statistics under pure fatigue by [22], as aforementioned in Section 2.1, a consistency can be found in terms of the major failure mode, i.e., Mode-3. However, opposite trend is found in the remain two modes due to the incorporation of corrosion effect.

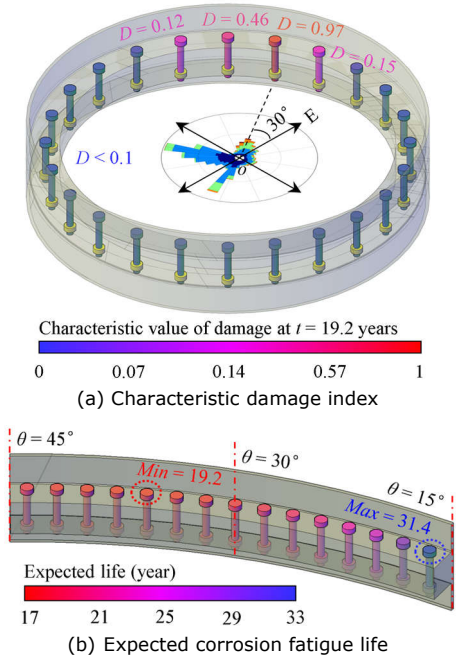

Figure 8 Characteristic value for the damage state of bolts.

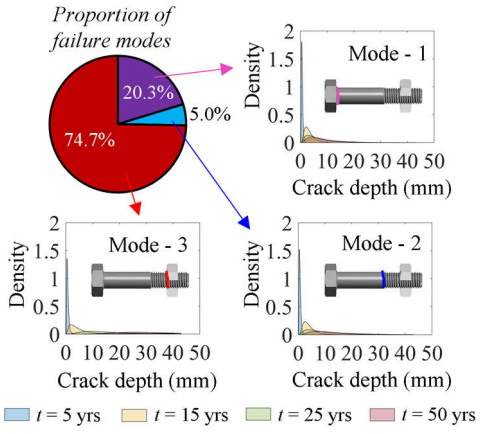

Figure 9 Major failure modes of bolts and associated crack growth.

Based on the evolution of probability distributions, the time-variant reliability curve is derived, as shown in Figure 10. In general, both the three failure modes demonstrate a non-linear decrease with time. Similarly, Model-2 (the run-off of threads) shows the highest reliability, followed by Mode-1 (the head-to-shank radius), while Mode-3 (the firstly engaged thread) reveals the lowest reliability. By

considering the limit of $\beta = 2$, the service life of the critical bolt is estimated as 19.2 years. It is worth noting that, if only Mode-3 is considered, a higher service life is predicted, i.e., 20.3 years. Meanwhile, in case of Mode-1, the service life increases beyond the design life of 25 years. Moreover, when only Mode-2 is accounted for, the beta index becomes well above the limit of 2 even after 30 years. To sum, although it is critical to identify the major failure mode of bolts under the C-F deterioration, the contribution by secondary modes is still apparent.

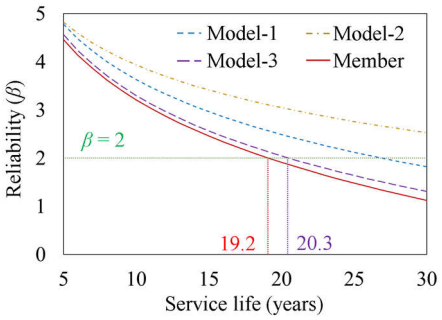

Figure 10 Reliability evolution of the critical bolt.

Further comparison is carried out between the corrosive and non-corrosive environment, as shown in Figure 11, to investigate the influence of environmental corrosion. Both the probability distribution and characteristic value (under survival rate of 97.7%) are derived. According to the result, the distribution of the C-F life transfer from a sharp one into a flat shape once the influence of corrosion is eliminated. As a consequence, the design life increases by almost 3 times.

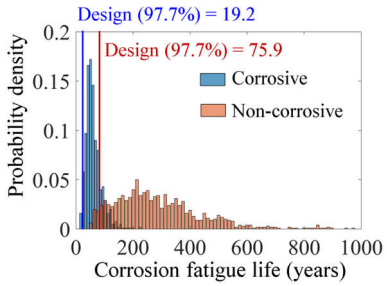

Figure 11 Distribution of corrosion fatigue life of the critical bolt.

4 Conclusion and future recommendation

This study integrates both the probabilistic corrosion fatigue (PCF) model, specific measurement of wind-wave and climate, and multi-physics simulation to perform a digital twin-based prognosis of C-F deterioration status of high-strength bolts in the ring-flange of wind turbine towers in a modular energy island (MEI). The major conclusions that can be drawn are listed below:

(1) A very apparent correlation is found between the wind-wave distribution and C-F states of bolts. The critical region is identified at the up-wind region of strong winds which is also the direction of the wind turbine. Thus, special attention is suggested based on the prognostic results.

(2) The high-strength bolts in a wind turbine tower on MEIs demonstrates 3 failure modes with different failure rates under the C-F deterioration. The firstly engaged thread shows the highest failure rate of 74.7%, followed by the head-to-shank radius of 20.3%, while the thread run-off suggests the lowest failure rate of 5.0%. Although it is crucial to identify the major failure mode, the contribution by remaining modes should also be included.

(3) The environmental corrosion risks a premature failure of bolts prior to the design life of 25 years. Under the reliability target of 2, the expected design life of the critical bolt becomes 19.2 years, i.e., 23% less than the design life. Thus, particular attention is recommended for high-strength bolts of wind turbine towers on MEIs.

(4) The digital twin-based prognosis present in this work not only offers a better understanding of bolt deterioration by integrating multi-source data and models, but also highlights the possibility for condition-based maintenance of wind turbine towers on MEIs. In the future work, a data-informed maintenance (DIM) plan is highly suggested based on the digital twin-based prognosis.

Acknowledgements

The Marie Curie Fellowship via URKI (EP/X022765/1), National Natural Science Foundation of China (52208182), COST Action MODENERLANDS (CA20109) and ROYAL SOCIETY (IES\R1\221036) and (IES\R1\211087) are gratefully acknowledged by the authors.

References

[1] European Commission (2019). A European Green Deal. Brussels, https://ec.europa.eu/info/strategy/priorities-2019-2024/european-green-deal_en

[2] European Commission (2020). Boosting Offshore Renewable Energy for a Climate Neutral Europe. https://ec.europa.eu/commission/presscorner/detail/en/IP_20_2096

[3] C.C.Baniotopoulos, C.Borri & E.Marino (eds) (2018), Wind Energy Harvestig...Focusing on the Exploitation of the Mediterranean Sea, Proceedings of the 2nd International WINERCOST and AEOLUS4FUTURE Conference, p. 344

[4] Watson, S., Moro, A., Reis, V., Baniotopoulos, C., Barth, S., Bartoli, G., ... & Wiser, R. (2019). Future emerging technologies in the wind power sector: A European perspective. Renewable and sustainable energy reviews, 113, 109270.

[5] UK Home Office, 2022. Policy paper: British energy security strategy. London, https://www.gov.uk/government/publications/british-energy-security-strategy/british-energy-security-strategy.

[6] Rebelo C., Modular Energy Islands for Sustainability and Resilience, Proceedings of "Coordinating Engineering for Sustainability and Resilience (CESARE'22)", 6-9 May, 2022. Jordan.

[7] Adedipe, O.;l Brennan, F.; Kolios, A. (2016). Review of corrosion fatigue in offshore structures: Present status and challenges in the offshore wind sector.

Renewable and Sustainable Energy Reviews, 61, 141-154.

[8] Stavridou, N., Efthymiou, E. & Baniotopoulos, C.C. (2015), Numerical Modelling of Welded Connec-tions of Wind Turbine Towers under Fatigue Loading, 8th GRACM International Congress on Computa-tional Mechanics, 12.07.-15.07.2015.

[9] Stavridou, N., Efthymiou, E. & Baniotopoulos, C.C. (2016), Wind Induced Fatigue in Wind Turbine Joints, 1st TU1304 WINERCOST 2016 Conference, Ankara 21.-22.04.2016.

[10] Viselli, A., Filippelli, M., Pettigrew, N., Dagher, H., & Faessler, N. (2019). Validation of the first LiDAR wind resource assessment buoy system offshore the Northeast United States. Wind Energy, 22(11), 1548-1562.

[11] Ozturk, G. B. (2021). Digital twin research in the AECO-FM industry. Journal of Building Engineering, 40, 102730.

[12] Opoku, D. G. J., Perera, S., Osei-Kyei, R., & Rashidi, M. (2021). Digital twin application in the construction industry: A literature review. Journal of Building Engineering, 40, 102726.

[13] Delgado, J. M. D., & Oyedele, L. (2021). Digital Twins for the built environment: learning from conceptual and process models in manufacturing. Advanced Engineering Informatics, 49, 101332.

[14] Jiang, F., Ma, L., Broyd, T., & Chen, K. (2021). Digital twin and its implementations in the civil engineering sector. Automation in Construction, 130, 103838.

[15] Boje, C., Guerriero, A., Kubicki, S., & Rezgui, Y. (2020). Towards a semantic Construction Digital Twin: Directions for future research. Automation in construction, 114, 103179.

[16] Chiachío, M., Megía, M., Chiachío, J., Fernandez, J., & Jalón, M. L. (2022). Structural digital twin framework: formulation and technology integration. Automation in Construction, 140, 104333.

[17] Pregnolato, M., Gunner, S., Voyagaki, E., De Risi, R., Carhart, N., Gavriel, G., ... & Taylor, C. (2022). Towards Civil Engineering 4.0: Concept, workflow and application of Digital Twins for existing infrastructure. Automation in Construction, 141, 104421.

[18] SAFETY4SEA (2019, November 19). Alexander L. Kielland: Norway’s worst offshore disaster. https://safety4sea.com/cm-alexander-l-kielland-norways-worst-offshore-disaster/?__cf_chl_jschl_tk__=pmd_H4dTRduGaTHxZ6DmDf98Uzca0si_upb.M2Vt.QD2k_Y-1632830550-0-gqNtZGzNAhCjcnBszQil

[19] Element (2021, May 21). Collapsed Wind Tower - A root cause investigation. www.element.com/nucleus/2021/collapsed-wind-tower

[20] Haselibozchaloee, D., Correia, J., Mendes, P., de Jesus, A., & Berto, F. (2022). A review of fatigue damage assessment in offshore wind turbine support structure. International Journal of Fatigue, 107145.

[21] Jawwad, A. K. A., ALShabatat, N., & Mahdi, M. (2021). The effects of joint design, bolting procedure and load eccentricity on fatigue failure characteristics of high-strength steel bolts. Engineering Failure Analysis, 122, 105279.

[22] Charlton, R. S. (2011, March). Threaded Fasteners: Part 1-Failure Modes And Design Criteria of Connections. In CORROSION 2011. OnePetro.

[23] Revie, R. W. (Ed.). (2011). Uhlig's corrosion handbook (Vol. 51). John Wiley & Sons.

[24] Zhang, Y., Zheng, K., Heng, J., & Zhu, J. (2019). Corrosion-fatigue evaluation of uncoated weathering steel bridges. Applied Sciences, 9(17), 3461.

[25] Liao, X., Qiang, B., Wu, J., Yao, C., Wei, X., & Li, Y. (2021). An improved life prediction model of corrosion fatigue for T-welded joint. International Journal of Fatigue, 152, 106438.

[26] Xiang, Y., & Liu, Y. (2010). EIFS-based crack growth fatigue life prediction of pitting-corroded test specimens. Engineering Fracture Mechanics, 77(8), 1314-1324.

[27] European committee for standardization (CEN), EN 1993: Eurocode 3 - design of steel structures, CEN, Brussels, Belgium, 2005.

[28] Liu, Y., & Mahadevan, S. (2009). Probabilistic fatigue life prediction using an equivalent initial flaw size distribution. International Journal of Fatigue, 31(3), 476-487.

[29] Hobbacher, A. F. (2016). Recommendations for fatigue design of welded joints and components (Vol. 47). Cham: Springer International Publishing.

[30] ISO. ISO 9223:2012(E) Corrosion of metals and alloys – Corrosivity of atmospheres – Classification, determination and estimation[S], ISO: Geneva, Switzerland, 2012.

[31] BSI. BS 7910 Guide to methods for assessing the acceptability of flaws in metallic structures[S], BSI: London, UK, 2015.

[32] ISO. ISO 9224:2021 Corrosion of metals and alloys — Corrosivity of atmospheres — Guiding values for the corrosivity categories, ISO: Geneva, Switzerland, 2012.

[33] ISO. ISO 9223:2012(E) Corrosion of metals and alloys – Corrosivity of atmospheres – Classification, determination and estimation, ISO: Geneva, Switzerland, 2012.

[34] National Data Buoy Center (NDBC), 2022. https://www.ndbc.noaa.gov/obs.shtml

[35] National Environmental Corrosion Platform (2023). National Materials Corrosion & Protection Data Center, https://www.corrdata.org.cn/index_en.php

[36] Hahin, C. (1994). Effects of corrosion and fatigue on the load-carrying capacity of structural and reinforcing steel (No. FHWA/IL/PR-108). Illinois, Dept. of Transportation. Bureau of Materials and Physical Research.

[37] Bak C., Zahle, F., Bitsche R., Kim T., Yde A., Henriksen L.C., Natarajan A. and Hansen M.H. (2013). Description of the DTU 10 MW Reference Wind Turbine. DTU Wind Energy Report-I-0092, Roskilde, Denmark.

[38] Gomez, P., S ´ anchez, G., Llana, A., Gonzalez, G., 2015. Qualification of innovative floating' substructures for 10MW wind turbines and water depths greater than 50m. https://cordis.europa.eu/project/id/640741

[39] National Renewable Energy Laboratory (NREL), 2022. OpenFAST – an open-source wind turbine simulation tool. https://github.com/openfast

[40] Weijtjens, W., Stang, A., Devriendt, C., & Schaumann, P. (2021). Bolted ring flanges in offshore-wind support structures-in-situ validation of load-transfer behaviour. Journal of Constructional Steel Research, 176, 106361.

[41] American Society for Testing and Materials (ASTM). (2017). Standard Practices for Cycle Counting in Fatigue Analysis (ASTM E1049-85). ASTM standards, West Conshohocken, PA, USA.